Lipid Flow through Fusion Pores Connecting Membranes of Different Tensions

Yuri A. Chizmadzhev,* Dimetry A. Kumenko,* Peter I. Kuzmin,* Leonid V. Chernomordik,# Joshua Zimmerberg,# and Fredric S. Cohen§

*Frumkin Institute of Electrochemistry, Moscow, Russia; #Laboratory of Cellular and Molecular Biophysics, National Institutes of Child Health and Human Development, National Institutes of Health, Bethesda, Maryland 20892 USA, and §Department of Molecular Biophysics and Physiology, Rush Medical College, Chicago, Illinois 60612 USA

ABSTRACT When two membranes fuse, their components mix; this is usually described as a purely diffusional process. However, if the membranes are under different tensions, the material will spread predominantly by convection. We use standard fluid mechanics to rigorously calculate the steady-state convective flux of lipids. A fusion pore is modeled as a toroid shape, connecting two planar membranes. Each of the membrane monolayers is considered separately as incompressible viscous media with the same shear viscosity, η_s. The two monolayers interact by sliding past each other, described by an intermonolayer viscosity, η_r. Combining a continuity equation with an equation that balances the work provided by the tension difference, $\Delta\sigma$, against the energy dissipated by flow in the viscous membrane, yields expressions for lipid velocity, υ, and area of lipid flux, Φ. These expressions for υ and Φ depend on $\Delta\sigma$, η_s, η_r, and geometrical aspects of a toroidal pore, but the general features of the theory hold for any fusion pore that has a roughly hourglass shape. These expressions are readily applicable to data from any experiments that monitor movement of lipid dye between fused membranes under different tensions. Lipid velocity increases nonlinearly from a small value for small pore radii, r_p, to a saturating value at large r_p. As a result of velocity saturation, the flux increases linearly with pore radius for large pores. The calculated lipid flux is in agreement with available experimental data for both large and transient fusion pores.

INTRODUCTION

The event that defines the fusion of two biological membranes is the formation of a fusion pore: a structural passageway linking two formerly separated aqueous spaces. Water-soluble materials move through this passageway; the membrane lipids may also move from one membrane to the other, but do so as a part of the pore walls themselves. The composition of the fusion pore at the time of formation is in dispute. Some hypothesize that the initial pore consists exclusively of protein (Tse et al., 1993; Lindau and Almers, 1995). Others argue that lipid is an essential component of the pore wall, along with protein (Zimmerberg et al., 1991; Nanavati et al., 1992; Chernomordik et al., 1995, 1997; Melikyan et al., 1995; Hernandez et al., 1996). If the initial pore is composed solely of protein, lipid could not move from one fusing membrane to the other until the pore enlarged. On the other hand, if the initial pore is a combination of lipid and protein, lipid movement between membranes could begin immediately upon pore formation, unless restricted by the proteins that contribute to pore structure. In any case, the larger a pore grows, the more one would expect lipid to move unhindered along the pore walls.

Diffusive movement of lipid along fusion pore walls has been analyzed in detail (Rubin and Chen, 1990; Chen et al., 1993). But if the two fusing membranes are under different tensions, lipid flux will be predominately convective rather than diffusive. There are experimental situations in which fusing membranes are known to be under different tensions. In the case of fusion of two planar membranes made from different lipids (Chernomordik et al., 1987), the tension difference is constant, it is independent of time, and it is maintained by the Gibbs-Plateau borders that support each planar membrane. When liposomes (Cohen et al., 1984) or cells (Melikyan et al., 1995) are fused to planar membranes, lipid will flow until the differences in tension that exist at the moment of fusion pore formation are relieved. Generally, liposomes are induced to swell—increasing their membrane tensions—to induce their fusion to planar membranes (Cohen et al., 1984; Niles et al., 1996) or to promote expansion of pores that form in the membrane shared by hemifused liposomes and planar bilayers (Chernomordik et al., 1995; Chanturiya et al., 1997). In some purely cellular situations, membranes may also be under different tensions as they fuse. In exocytotic fusion, careful measurements that have tracked lipid movement during pore flickering—the opening and closing of small pores—suggest that the exocytotic granule membranes are under significantly more tension than plasma membranes (Monck et al., 1990; Solsona et al., 1998). It may be that tension-driven membrane flow after fusion is more common than currently appreciated: membrane tension, for example, appears to strongly promote postfusion convective flow of Golgi membrane into endoplasmic reticulum membrane (Sciaky et al., 1997).

In this study, we use the equations of fluid mechanics to describe lipid flow through a fusion pore of constant size

Received for publication 28 September 1998 and in final form 31 March 1999.

Address reprint requests to Dr. Fred S. Cohen, Department of Molecular Biophysics and Physiology, Rush Medical College, 1653 W. Congress Parkway, Chicago, IL 60612-3864. Tel.: 312-942-6753; Fax: 312-942-8711; E-mail: fcohen@rush.edu.

0006-3495/99/06/2951/15 $2.00

joining two membranes under different tensions. The calculated flux agrees with measured values (Monck et al., 1990; Melikyan et al., 1995). Experimentalists who wish to analyze data of transfer of lipid dye observed during fusion can use the graphs of Fig. 2, and Eqs. 20 and 21, which describe lipid velocity and area flux, to calculate differences in membrane tensions. This calculation requires reasonable estimates of membrane viscosity and a knowledge of pore radii, which can be obtained from simultaneous electrophysiological measurements of fusion pore conductance.

STATEMENT OF THE PROBLEM

The geometry of the system

Consider two parallel planar membranes, each of thickness $2h$, whose neutral surfaces (the interfaces between the two monolayers) are separated by $2H$ (Fig. 1 *A*). A fusion pore of toroidal shape (a half-circle revolved around the z axis) connects the planar bilayers. The system is cylindrically symmetrical about the z axis, which passes through the center of the pore. We define the distance from the z axis to the boundary between the toroidal and unbent planar surfaces as the pore radius, R. The radius of the narrowest portion of the lumen of the pore is $r_p = R - (H + h)$. It is obvious that $r_p \geq 0$ and $R \geq (H + h)$. The radius of the fusing objects is given by $R_m \gg R$. The symbols σ_1 and σ_2 designate tensions of single monolayers in the upper (1) and lower (2) membranes (Fig. 1 *A*). We consider the case when the monolayers of a given membrane are under the same tension, and the two bilayer tensions are different, $2\sigma_1 > 2\sigma_2$, maintained as a constant at the circumference R_m. The geometry of the planar portions of the membranes is described by cylindrical coordinates (r, z, θ), where r is measured relative to the z axis (Fig. 1 *B*). For the toroidal portion, we use the more specialized coordinates (θ, φ, ρ) (Fig. 1, *A* and *B*). The ρ coordinate takes on values within an interval $H + h > \rho > H - h$. The angle φ is confined in the interval $[-\pi/2, \pi/2]$ and is equal to zero on the equatorial plane. The azimuthal angle θ is defined in the interval $[0, 2\pi]$. To calculate lipid flow induced by differences in membrane tension, we assume that a fusion pore maintains its shape and dimension (i.e., all geometrical parameters R, H, h as well as the tensions σ_1 and σ_2 remain constant). For fusion systems in general (e.g., cell-cell fusion or exocytotic fusion), for pore radius R, much smaller than the characteristic size of the fusing objects, the two fusing membranes can be treated as planar and parallel to each other, connected by a pore.

Fluid mechanical approach

In biological membranes, lipids form a continuous fluid phase. The presence of proteins affects lipid dynamics through changes in membrane viscosity. Artificial lipid bilayers as well as cell membranes are essentially anisotropic systems, with lipid mobility restricted to the plane of the membrane. Lipid does not move normal to the plane of the membrane, but within the plane flows as a liquid. Bilayer membranes can be characterized as a mechanical continuum with material properties such as an elastic modulus and coefficient of viscosity (Evans and Skalak, 1980); volumetrically they are almost incompressible (Evans and Hochmuth, 1978; Nagle and Wilkinson, 1978).

In this paper we rigorously calculate the stationary convective flux of lipids by using standard fluid mechanics: for stationary convective flow, the work performed by the tension difference to cause lipid movement is balanced by the dissipation of mechanical energy due to viscosity. Dissipation of energy that accompanies lipid flow occurs because

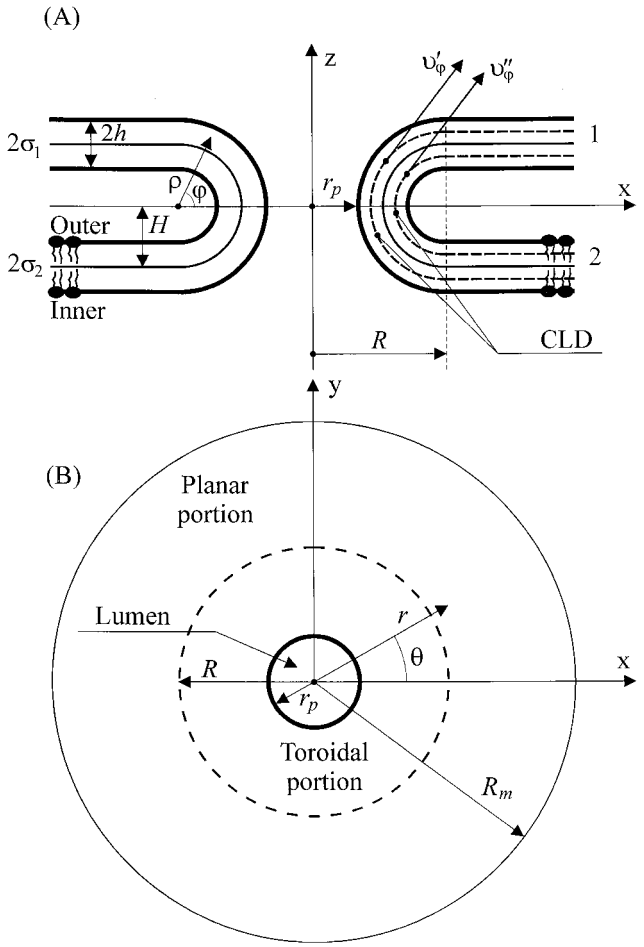

FIGURE 1 Schematic representation of a toroidal fusion pore connecting two planar membranes, 1 and 2, at different tensions, $2\sigma_1$ and $2\sigma_2$, with $2\sigma_1 > 2\sigma_2$. (*A*) Cross-sectional, side view of the system in z, x coordinates. The bold solid lines represent membrane-solution interfaces. The surfaces of constant lipid density (CLD) for each monolayer are shown as dashed lines. The velocities defined on these surfaces, υ'_φ and υ''_φ, are shown by arrows. The thin solid lines designate the interfaces between monolayers. (*B*) Top view of the system in y, x coordinates. The walls of the toroidal pore meet the planar membranes at radius R. The radius of the narrowest portion of the water-filled pore lumen is given by r_p. Thus the toroidal part of the membrane lies between r_p and R. The coordinate systems (x, y, z), (r, θ, z), and (ρ, φ, θ) illustrated here are described in the main text and in Appendix A.

of two types of deformation: in-plane shear and relative sliding of monolayers. Dissipation due to shear deformations in both the planar membrane and toroidal pore originates from lipid-lipid and lipid-protein interactions within each monolayer. These intermolecular interactions are described with a shear viscosity, η_s. Dissipation due to relative movement of monolayers arises from viscous friction between the monolayer leaflets as they slip past each other and is described with a relative viscosity, η_r. The viscous friction between a monolayer and the bathing aqueous solution is negligibly small (see Discussion).

We calculate lipid flow by first solving the equations of fluid mechanics within both the planar membranes and the curved toroidal pore and then matching their solutions at the boundaries where they join. For planar membranes, flow is purely radial and for an incompressible viscous monolayer is easily calculated (Deryaguin and Gutop, 1962; Deryaguin and Prokhorov, 1981). The situation for a curved toroidal membrane is more complicated. Within the inner monolayer of a toroidal pore (Fig. 1 *A*), the area available to a lipid headgroup is greater than that available to the acyl chains. In this monolayer, therefore, the region occupied by the headgroups is expanded relative to the portion filled by the acyl chains, which is compressed. The opposite consideration pertains to the outer monolayer. This means that a curved monolayer of finite thickness does not strictly have constant density. Attempts to account for nonconstant density lead to horrendous mathematical complexities. We avoided this problem by choosing within each monolayer of the toroidal pore a surface of constant lipid density (CLD) that matches the lipid density (molecules/unit area) of the planar membranes (Fig. 1 *A*). This surface lies between the polar headgroups and the hydrophobic acyl chains. By considering surfaces of CLDs instead of monolayers of finite thickness, the fluid mechanical problem is reduced to a two-dimensional problem of the flow of an incompressible liquid along these surfaces. We explicitly consider frictional interactions between the two surfaces of the CLD. For calculational concreteness, we assume that each surface of CLD is located in the middle of its monolayer (i.e., at $\rho = H \pm h/2$) and has a toroidal geometry within the fusion pore.

THEORY

Velocity distribution

The radial flow of lipid in the planar portions of the membrane is obtained from the condition that membranes are incompressible. We write this conservation of area as an equation of continuity:

$$\Phi' = 2\pi r \cdot v_r' = \text{const.}', \quad \Phi'' = 2\pi r \cdot v_r'' = \text{const.}'' \tag{1}$$

where r is an arbitrary radius on the plane, Φ is area flux, and v_r is the velocity at r. The superscripts $'$ and $''$ denote the surfaces of CLD of the inner and outer monolayers, respectively. We rewrite Eq. 1 as

$$rv_r' = Rv', \quad rv_r'' = Rv'' \tag{1'}$$

where R is a pore radius (Fig. 1), and v' and v'' are the linear velocities of lipid in the two monolayers at $r = R$, the junction of the toroidal pore and planar membranes. The constants v' and v'' must be determined.

We use the same principle of continuity of area flux to obtain lipid velocities on the toroidal surface of the pore. For reasons of symmetry, only the φ-component of the velocity v_φ is nonzero (see Fig. 1 *A*):

$$\Phi' = 2\pi r' v_\varphi' = \text{const.}', \quad \Phi'' = 2\pi r'' v_\varphi'' = \text{const.}'' \tag{2}$$

where $r' = R - (H + h/2)\cos\varphi$ (Eq. A9 when $\rho = H + h/2$) is the radius of the surface of the CLD of the inner monolayer of the toroidal pore at angle φ. For the outer CLD surface we have $r'' = R - (H - h/2)\cos\varphi$. It is convenient to rewrite Eq. 2 in the form

$$r'v_\varphi' = Rv', \quad r''v_\varphi'' = Rv'' \tag{2'}$$

where v' and v'' are the constants (linear velocities at $r = R$) of Eqs. 1′ and 2′. These equations define the velocity distributions in the planar and toroidal portions of outer and inner monolayers:

$$\begin{aligned} v_r'' &= \frac{v'' R}{r} && \text{planar part} \\ v_\varphi'' &= \frac{v'' R}{R - (H \pm h/2)\cos\varphi} && \text{toroidal part} \end{aligned} \tag{3}$$

where + and − signs correspond to the inner (′) and outer (″) monolayers, respectively. These equations are valid for the upper (denoted 1, Fig. 1) and lower (2) membranes, but an essential asymmetry should be noted. If the tension is larger in the upper than in the lower membrane, $2\sigma_1 > 2\sigma_2$, lipid flows from the lower to the upper membrane. So that lipid velocities have the same sign in membranes 1 and 2, we assign a positive direction for flow toward the z axis in membrane 2 and away from the z axis in the upper membrane 1. In the toroidal pore, the velocity v_φ is directed from $\varphi = -\pi/2$ to $\varphi = \pi/2$. Equation 3 shows that v_φ achieves a maximum value at $\varphi = 0$.

To obtain the velocity distributions everywhere in the system, we need only to determine the two unknown parameters, v' and v''. This is obtained rigorously by using a local balance of force equation for each monolayer, valid when flow has reached steady state. Balancing tension by the opposing viscous forces yields two equations for the two unknown constants v' and v''. These calculations are presented in Appendix B, where it is shown that for $R_m \gg R$, the two monolayers move almost together in the planar portions of the system, without relative sliding. That is, to a reasonable approximation, $v_r' = v_r''$ at any r, and therefore

$$v' = v'' = v \tag{4}$$

The physical reason Eq. 4 holds is that if monolayers were to slide past each other over the large area covered by the planar membranes ($R < r < R_m$), the energy dissipation would be enormously high. This would contradict the prin-

ciple that entropy production is at a minimum for stationary states (Prigogine, 1967). Minimum entropy production occurs when monolayers only slide past each other within the walls of the toroidal pore, a much smaller area than is covered by the planar portions of the system.

The approximation of Eq. 4 significantly simplifies the problem. The velocity distribution in the whole system is defined by the single parameter v, the lipid velocity at $r = R$ (i.e., $v = v_r(R)$). We find v by using the energy balance equation for the whole membrane (which is computationally more convenient than employing an equation of local force balance). With the approximation of Eq. 4 we can rewrite the velocity distribution, Eq. 3, in the simple form:

Inner monolayer

$$\begin{cases} v'_r = \dfrac{vR}{r} & \text{planar part} \\ v'_\varphi = \dfrac{vR}{R - (H + h/2)\cos\varphi} & \text{toroidal part} \end{cases} \quad (3')$$

Outer monolayer

$$\begin{cases} v''_r = \dfrac{vR}{r} & \text{planar part} \\ v''_\varphi = \dfrac{vR}{R - (H - h/2)\cos\varphi} & \text{toroidal part} \end{cases}$$

It is clear from Eq. 3′ that at any r, lipid velocities of both monolayers are the same in the planar portions of the system ($v'_r = v''_r$). But in the toroidal portion, lipid velocities in inner monolayers are greater than in outer ones, $v'_\varphi \geq v''_\varphi$, because lipid traverses a longer pathway in the inner monolayer than in the outer monolayer (Fig. 1 *A*). At the junction between the planar and toroidal portions, $\varphi = \pm\pi/2$, $r = R$, the values of all velocities coincide, $v_r(R) = v'_\varphi(\pm\pi/2) = v''_\varphi(\pm\pi/2) = v$, in accord with the original continuity equations.

The energy balance condition for the entire membrane system sets the work done by the tension forces per unit of time, $\dot{W}_\sigma$, equal to the rate of energy dissipation, $\dot{E}$:

$$\dot{W}_\sigma = \dot{E} \quad (5)$$

Evaluating and equating the functions $\dot{W}_\sigma$ and $\dot{E}$ determine v. This allows the area of lipid flux to be obtained.

The work of tension forces

The work per unit time produced by tension (force/unit length) acting on the (1) upper bilayer and (2) lower bilayer is equal to the product of the force acting on the membrane boundary, $r = R_m$, of circumference $2\pi R_m$ and the velocity of the boundary v_m. For the upper bilayer,

$$\dot{W}_{\sigma 1} = 2\sigma_1 \cdot 2\pi R_m \cdot v_m \quad (6)$$

and for the lower bilayer,

$$\dot{W}_{\sigma 2} = -2\sigma_2 \cdot 2\pi R_m \cdot v_m \quad (7)$$

The minus sign in Eq. 7 arises from the fact that for the case $\sigma_1 > \sigma_2$, lipid in bilayer (2) moves in a direction opposite that of the applied tension, σ_2.

We obtain v_m through the velocity distribution, Eq. 3′:

$$v_m = \frac{v \cdot R}{R_m} \quad (8)$$

Combining Eqs. 6, 7, and 8, we obtain the total work performed by tension forces per unit time:

$$\dot{W}_\sigma = \dot{W}_{\sigma 1} + \dot{W}_{\sigma 2} = 4\pi R \Delta\sigma v \quad (9)$$

where $2\Delta\sigma = 2\sigma_1 - 2\sigma_2$.

Energy dissipation

We assume that only viscous forces dissipate energy. For example, we consider bending of an element of a membrane that enters the toroidal region a reversible elastic process without an accompanying dissipation. The energy dissipation in the membrane per unit time, $\dot{E}$, therefore consists of three terms:

$$\dot{E} = \dot{E}_{sp} + \dot{E}_{st} + \dot{E}_{rt} \quad (10)$$

The first term refers to viscous dissipation due to shear deformation within a single monolayer (s) in the planar (p) portions of the membranes; the second term describes the same process, but within the toroidal (t) pore. We refer to dissipation due to friction within a monolayer as intramonolayer dissipation. The third term denotes dissipation induced by relative (r) motion of monolayers past each other in the toroidal (t) pore, intermonolayer dissipation. As discussed, monolayers do not slide past each other in the planar portions ($v' = v''$), and hence there is no dissipation in this region through friction between monolayers. But as there is sliding between monolayers in the toroidal pore, it is important that each monolayer be considered separately.

As a direct consequence of the Navier-Stokes equations of fluid mechanics, the energy dissipated when an incompressible viscous fluid is deformed by shear can be written as (Landau and Lifshitz, 1987)

$$\dot{E}_s = \frac{1}{2\eta_s} \sum_{j,k} \int \sigma_{jk}^2 dS \quad (11)$$

where η_s is the two-dimensional shear (intramonolayer) viscosity, σ_{jk} is the viscous stress tensor, and dS is the element of the surface. Substituting dS and σ_{jk} in cylindrical coordinates (Eqs. A4 and A5) into Eq. 11 yields for the planar portions

$$\dot{E}_{sp} = 16\pi\eta_s v^2 \quad (12)$$

The shear dissipation within the toroidal pore, $\dot{E}_{st}$, is also determined by Eq. 11, with dS and σ_{jk} given by Eqs. A8 and A10:

$$\dot{E}_{st} = 8\pi\eta_s\tilde{I}(b)v^2 \tag{13}$$

where

$$\tilde{I}(b) = 2\int_{-\pi/2}^{\pi/2} \frac{b^2\sin^2\varphi\, d\varphi}{(b-\cos\varphi)^3}, \quad b = \frac{R}{H}. \tag{14}$$

Equation 13 was obtained under the assumption that bilayer thickness $2h$ is small compared with the distance between membranes $2H$ ($h/H \ll 1$). $\tilde{I}(b)$ is a geometrical dimensionless factor determined by the shape of the pore. The expressions for $\dot{E}_{sp}$ (Eq. 12) and $\dot{E}_{st}$ (Eq. 13) are similar, arising from the same physics, and differ only by the geometrical factor $\tilde{I}(b)$.

Energy dissipation due to relative motion of monolayers in the toroidal pore, $\dot{E}_{st}$, is physically attributed to the friction between the methyl-terminal portions of the acyl chains of the phospholipids that arise when the two monolayers slide against each other. According to membrane mechanics, such dissipation is described as (Evans and Hochmuth, 1978)

$$\dot{E}_{rt} = \mu\int(\Delta v)^2 dS \tag{15}$$

where μ is a friction coefficient and Δv is the velocity difference between the two monolayers at the interface over which the integration is carried out. To obtain linear velocities, we calculate angular velocities, $\Omega(\varphi)$, for each monolayer. For the surface of CLD of the inner monolayer,

$$\Omega'(\varphi) = \frac{v'_\varphi}{H + h/2} \tag{16}$$

$\Omega'(\varphi)$ is a function of $v'_\varphi(\varphi)$, in turn given by Eq. 3′. A similar expression holds for the outer monolayer:

$$\Omega''(\varphi) = \frac{v''_\varphi}{H - h/2} \tag{16′}$$

The friction between monolayers can be formally described as two surfaces of CLD sliding past each other. But to provide a physical appreciation of this friction, we treat lipid molecules as rigid rods that remain perpendicular to the neutral surface of the bilayer (i.e., the interface between the two monolayers) as they move along the toroid. For the lipids-as-rods simplification, the angular velocities of each monolayer (Eqs. 16 and 16′) at their surface of interaction ($\rho = H$) immediately yields linear velocities $v_\varphi(\rho = H)$ at this surface:

$$v'_\varphi(H) = \frac{v'_\varphi}{H + h/2}\cdot H, \quad v''_\varphi(H) = \frac{v''_\varphi}{H - h/2}\cdot H \tag{17}$$

The difference between $v'_\varphi(H)$ and $v''_\varphi(H)$ provides Δv, as needed in Eq. 15. For $h/H \ll 1$, substituting the velocity profiles of Eq. 3′ into Eq. 17 allows the integration of Eq. 15 to be performed, yielding

$$\dot{E}_{rt} = 8\pi\eta_r J(b)v^2, \quad \eta_r = \mu h^2 \tag{18}$$

where

$$J(b) = \frac{1}{4}\int_{-\pi/2}^{\pi/2} \frac{b^2(b-2\cos\varphi)^2}{(b-\cos\varphi)^3}\, d\varphi \tag{18′}$$

is a dimensionless geometric factor, and $\eta_r = \mu h^2$ is a two-dimensional relative viscosity. The monolayer thickness, h, appears as a scaling parameter between η_r and μ as a direct consequence of our conceptualization of lipids as rods. But as the surfaces of CLDs are separated by a distance h, the scaling parameter is a general one, appearing routinely in membrane mechanics (Evans and Hochmuth, 1978).

$\dot{E}_{sp}$ (Eq. 12), $\dot{E}_{st}$ (Eq. 13), and $\dot{E}_{rt}$ (Eq. 18) have the same forms. Each term varies quadratically with v, differing only in their geometrical "form factors." The total energy of dissipation is obtained by substituting Eqs. 12, 13, and 18 into Eq. 10:

$$\dot{E} = 8\pi[\eta_s I(b) + \eta_r J(b)]v^2, \quad I(b) = 2 + \tilde{I}(b) \tag{19}$$

The form factor $I(b)$ describes the effect of the geometries of the two planar membranes (the first term, 2) and the toroidal pore (the second term, $\tilde{I}(b)$) as they contribute to energy dissipation that occurs through shear viscosity. $J(b)$ is the geometrical factor contributed by the toroidal shape to intermonolayer energy dissipation. The geometrical factors $I(b)$ (Eq. 14) and $J(b)$ (Eq. 18) are illustrated in Fig. 2 and enumerated in Table 1 for $H = 10$ nm and $h = 2$ nm. Their asymptotic forms for $b \gg 1$ and $b \to 1$ are presented in Table 2. $I(b)$ monotonically decreases toward 2 (2 is the contribution from the planar membranes) as $b \to \infty$. That is, as the pore enlarges, it contributes progressively less to shear dissipation (i.e., $\tilde{I}(b) \to 0$). The factor $J(b)$ is biphasic, at first decreasing sharply for increasing r_p, descending to a minimum at $b \approx 2$ ($r_p \approx 5$ nm) and then slowly increasing with a constant slope of $\pi/4$. $I(b) > J(b)$ over the entire range of pore radii, up to $r_p \approx 35$ nm. For large pores, the inequality reverses, $J(b) > I(b)$. The energy dissipation rate (Eq. 19) depends not only on $I(b)$ and $J(b)$, but on the viscosities η_s and η_r as well. We consider the values of shear and intermonolayer viscosities in the Discussion. This allows us to evaluate the relative contributions of the two processes to energy dissipation that determine lipid flux.

Lipid velocity and area flux

Substituting the expressions for the work performed by tension (Eq. 9′) and the energy dissipated by lipid flow (Eq.

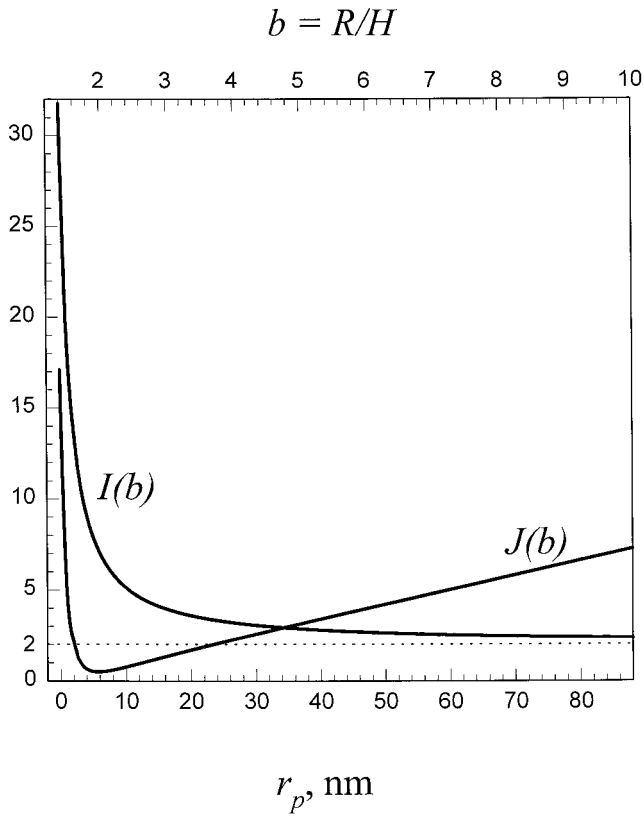

FIGURE 2 The dependence of the geometrical factors $I(b)$ and $J(b)$ on the radius of the pore lumen r_p and on $b = R/H$ for $H = 10$ nm. The dashed line (ordinate = 2) is the geometric contribution that the planar membranes makes to shear dissipation and is independent of the size of the pore.

19) into the energy balance equation (Eq. 5), we obtain

$$4\pi R\Delta\sigma\upsilon = 8\pi[\eta_s \cdot 2 + \eta_s\tilde{I}(b) + \eta_r J(b)]\upsilon^2 \qquad (5')$$

This equation yields the parameter υ, the lipid velocity at $r = R$:

$$\upsilon = \frac{\Delta\sigma R}{2[\eta_s I(R/H) + \eta_r J(R/H)]} \qquad (20)$$

Substituting this expression for υ into Eq. 3′ yields the velocity distributions

$$\upsilon_r = \frac{\Delta\sigma R^2}{2r[\eta_s I(R/H) + \eta_r J(R/H)]} \quad \text{planar part} \qquad (20')$$

$$\upsilon'_\varphi = \frac{\Delta\sigma R^2}{2[\eta_s I(R/H) + \eta_r J(R/H)]} \cdot \frac{1}{R - \left(H + \frac{h}{2}\right)\cos\varphi}$$

$$\upsilon''_\varphi = \frac{\Delta\sigma R^2}{2[\eta_s I(R/H) + \eta_r J(R/H)]} \cdot \frac{1}{R - \left(H - \frac{h}{2}\right)\cos\varphi}$$

toroidal part

The area flux for a bilayer, calculated at $r = R$, follows directly from Eq. 20:

$$\Phi = \frac{2\pi\Delta\sigma R^2}{[\eta_s I(R/H) + \eta_r J(R/H)]} \qquad (21)$$

where the 2 in the numerator arises because there are two monolayers per bilayer. We have thus arrived at equations for υ and Φ as a function of pore radius R, intermembrane distance H, tension difference $\Delta\sigma$, and the viscosities η_s, η_r.

Fig. 3, *A* and *B*, illustrates the dependence of velocity at the junction between the planar membranes and the toroidal pore, $\upsilon(b)$, on pore size. Pore size is shown as both $b = R/H$ and as the radius of the narrowest portion of lumen, r_p. Fig. 3 *A* displays $\upsilon(b)$ over an extensive range of pore radii; Fig. 3 *B* exhibits this velocity at greater resolution for pores with small radii. The corresponding figures for the flux, $\Phi(b)$, are presented in Fig. 4, *A* and *B*. Both $\upsilon(b)$ and $\Phi(b)$ are plotted on the left-hand ordinates for the parameters $H = 10$ nm, $h = 2$ nm, $\Delta\sigma = 0.1$ dyn/cm, and $\eta_s = \eta_r = 10^{-5}$ g/s. The right-hand ordinates of both Figs. 3 and 4 show the dimensionless combinations $\upsilon\eta/\Delta\sigma H$ and $\Phi\eta/\Delta\sigma H^2$. This allows us to readily obtain υ and Φ from Figs. 3 and 4 for any values of η, $\Delta\sigma$, and H.

DISCUSSION

When fusing membranes are at different tensions, convective flow of lipid occurs through the wall of the fusion pore. This flow is governed by the principle that in steady state, the energy per unit time supplied by the tension is balanced by the viscous dissipation caused by the flow. We calculated flow by treating a membrane as a two-dimensional homogeneous continuum (Evans and Skalak, 1980). The approach of treating a membrane as a continuum is certainly valid when distance scales are on the order of 0.1 μm or greater. However, equations that are strictly correct only in macroscopic limits have long been successfully applied to phenomena that occur over microscopic scales (Einstein, 1956). In the field of membrane fusion, macroscopic membrane mechanics (Helfrich, 1973) has been of value when applied to curved surfaces of 10-nm scale, such as pores or stalks (Markin et al., 1984; Nanavati et al., 1992; Siegel, 1993).

In exocytotic secretion, as observed by electron microscopy, fusion is initiated by dimpling of membranes toward each other (Chandler and Heuser, 1979; Ornberg and Reese, 1981; Knoll et al., 1991; Curran et al., 1993). Once formed, fusion pores are long structures with nonuniform luminal radii (Curran et al., 1993). Based on functional studies of virus-induced fusion, even small flickering pores already have a length greater than the thickness of a bilayer membrane (Razinkov et al., 1998). A toroidal shape captures the essential geometrical features of biological fusion pores—a significant length with a narrow luminal region over part of it. Choosing an explicit geometry to model pore shape allows for rigorous calculations, which in turn leads to a

TABLE 1 The values of geometric factors $I(b)$ and $J(b)$ at different $b = R/H$ and r_p

b	1.2	1.3	1.4	1.6	1.8	2.0	2.2	2.4	2.6	2.8	3.0	5.0	10
r_p (nm)	0	1	2	4	6	8	10	12	14	16	18	38	88
$I(b)$	31.77	19.34	13.95	9.18	7.07	5.89	5.15	4.64	4.27	3.99	3.77	2.84	2.23
$J(b)$	17.12	5.14	2.07	0.66	0.51	0.61	0.78	0.96	1.15	1.34	1.52	3.24	7.80

more intuitive understanding of the general qualitative features of the process of lipid flow. The lipid velocity υ (Eq. 20) and lipid area flux Φ (Eq. 21) depend, in physically understandable terms, on the tension difference, $\Delta\sigma$, between the two fusing membranes and on their shear and relative viscosities, η_s and η_r, as well as geometrical factors. We consider appropriate values for η_s and η_r and then discuss the contributions that shear deformation and intermonolayer friction make to energy dissipation in view of the geometrical aspects of fusion pores. The underlying basis for the functional dependence of lipid velocity and flux on pore radius is also considered. Finally, we show that the theoretical equations can account for the experimental data currently available.

We have rigorously calculated the steady-state lipid flux for fused lipid membranes under the conditions that $\Delta\sigma$ and pore radius R remain constant. We apply the equations to biological membranes by using values of η_s and η_r that are appropriate for these membranes. In experimental practice, sizes of fusion pores are never perfectly constant, although they often tend to remain reasonably stable for extended times before enlarging significantly. In any case, lipid fluxes quickly reach steady state (instantaneously compared to the video rates for which they are measured). The time, τ, needed for a tension difference to establish steady-state flux can be estimated from the Navier-Stokes equation for an incompressible liquid (Landau and Lifshitz, 1987) as $\rho R^2/\eta$, where ρ is lipid density. For $\eta = 10^{-5}$ g/s, $\rho = 10^{-5}$ g/cm^2, and $R = 100$ nm, $\tau = 10^{-10}$ s. For a compressible liquid, τ can be approximated as the time needed for sound (velocity $\approx 10^5$ cm/s) to propagate over the entire object. For a cell of radius 10 μm, $\tau \approx 10^{-8}$ s. The equations of this study, assuming constant pore radius, therefore allow lipid fluxes to be calculated at every instant, even if pore size varies significantly (size determined from electrophysiological measurements).

Membrane tension

The basis for tension in planar membranes is well understood: lipids within the planar bilayer and the supporting Gibbs-Plateau border have different chemical potentials, creating a tension difference. Planar bilayer tensions lie in the range of 0.2–4 dyn/cm, the precise number depending on lipid and aqueous compositions (Tien, 1974; Chernomordik et al., 1987). Biological membranes are also under tension. Plasma membranes of eukaryotes have tensions that arise from both interactions between constituents within the plane of the membrane itself and from interactions between the plasma membrane and cytoskeleton. But these tensions are significantly less than for planar membrane: the in-plane tension of a plasma membrane is only $\sim 10^{-2}$ dyn/cm if the cell is not osmotically stressed (Dai and Sheetz, 1995a), and hence the lateral lipid flow between fused plasma membranes should be small. It also appears that membranes of internal organelles are under tension, to a greater degree than plasma membranes. From measured redistribution of chimeras consisting of a membrane protein and green fluorescent protein, it has been concluded that movement of membrane protein between ER and Golgi is due to convective flow, rather than diffusive movement, with velocities on the order of 10 μm/s (Sciaky et al., 1997). Differences between chemical potentials of ER and Golgi membranes are presumably responsible for tension differences. It would thus be expected that in many cellular processes involving organelles, lipid movement could be due to convective flow, rather than diffusive spread, as is often assumed. For example, there is significant lipid flux through fusion pores from plasma to granule membrane in mast cell secretion (Oberhauser and Fernandez, 1993), implying that the granules are under significant tension (Monck et al., 1990).

TABLE 2 Asymptotic expressions for the geometrical factors $I(b)$ and $J(b)$

	$b - 1 \ll 1$	$b \gg 1$
$I(b)$	$\frac{\pi}{\sqrt{2}}\frac{1}{(b-1)^{3/2}}$	2
$J(b)$	$\frac{3\pi}{16\sqrt{2}}\frac{1}{(b-1)^{5/2}}$	$\frac{\pi b}{4}$

Membrane viscosity

As lipid flow depends on η_s and η_r, their values are required to compare the theoretical equations with available experimental data. The values of shear viscosities reflect molecular interactions and differ for different types of membranes (lipid bilayers, lipid monolayers, and cell membranes); these values lie in a very broad interval, 10^{-7} g/s $< \eta_s <$ 10^{-3} g/s (Evans and Hochmuth, 1978). The surface viscosity of a membrane can be converted to a three-dimensional viscosity, $\eta_3 = \eta_s/h$, and compared to viscosities of common substances. The largest surface viscosity value (10^{-3} g/s) compares with the three-dimensional viscosity of extremely viscous materials such as waxes and butter ($\eta_3 = 10^4$ poise, i.e., 10^4 g/s $\cdot$ cm). These large values are found in experiments that deform extended portions of a cell membrane. Such high values probably reflect additional forces

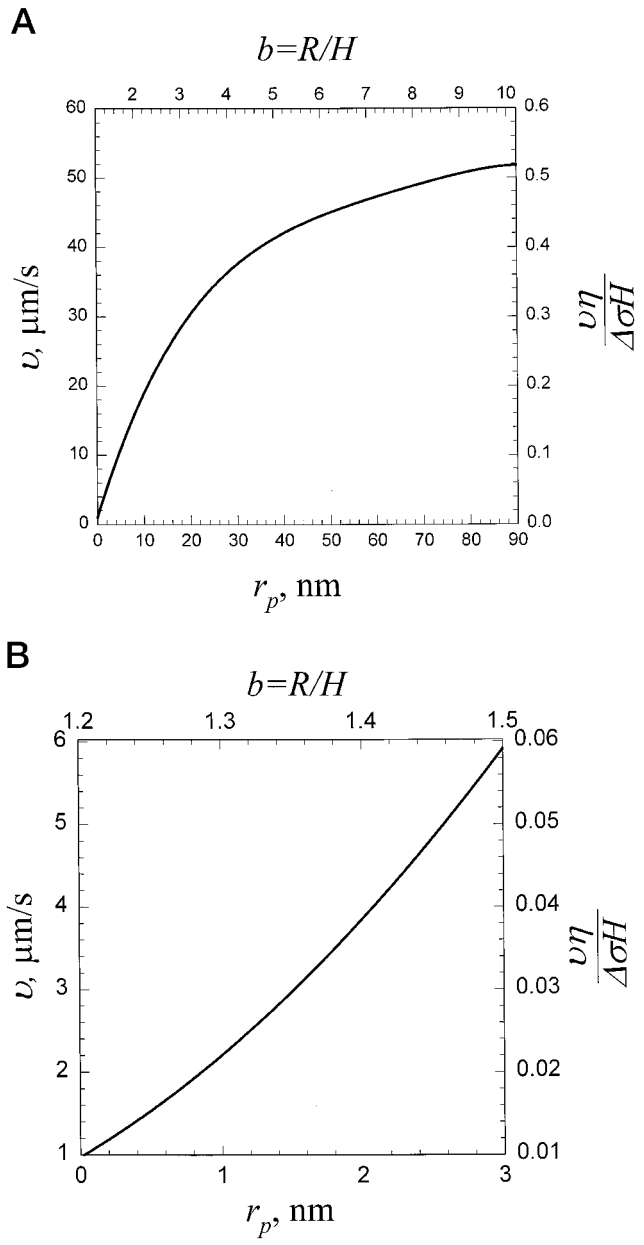

FIGURE 3 The dependence of an average lipid velocity υ on the radius of the pore lumen, r_p, and on the dimensionless pore radius, $b = R/H$. The curve is plotted for $H = 10$ nm, $\eta_s = \eta_r = \eta = 10^{-5}$ g/s, and $\Delta\sigma = 0.1$ dyn/cm. The left-hand ordinate gives υ in absolute units, and the right-hand ordinate gives velocity in dimensionless units. This allows υ to be readily obtained for any values of η, $\Delta\sigma$, and H. (*A*) Velocity is shown over a large range of pore radii. (*B*) Velocity is presented over the range of narrow pores.

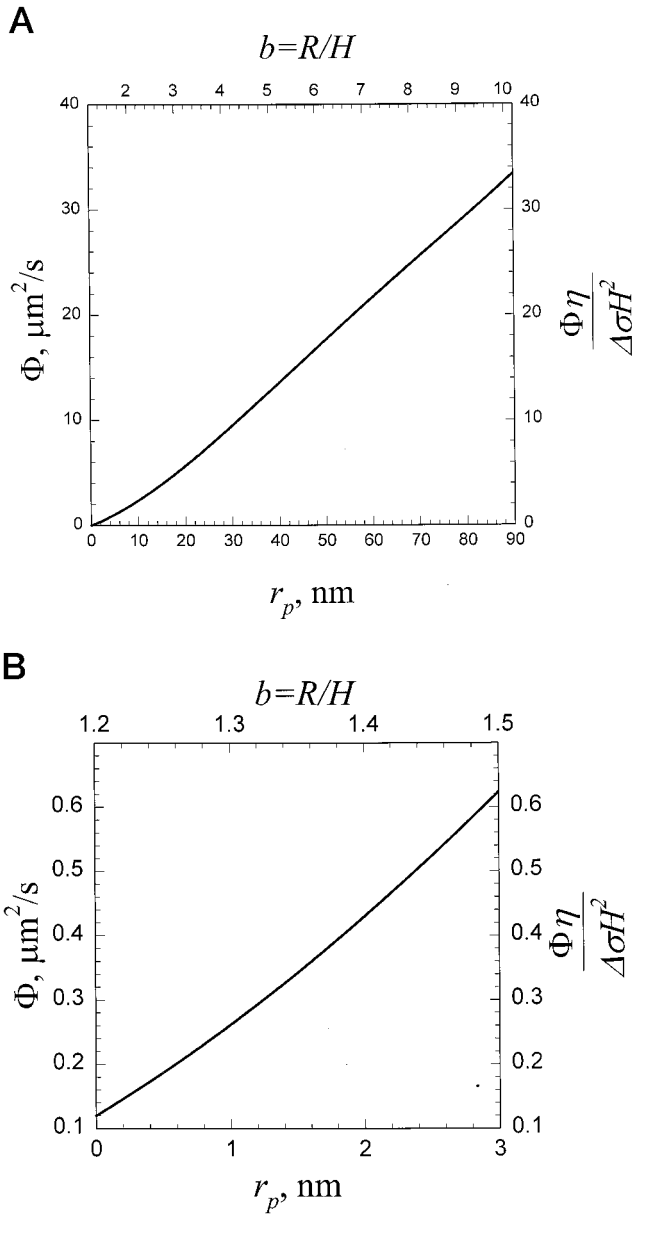

FIGURE 4 The dependence of lipid area flux Φ on pore lumen radius r_p and on the dimensionless pore radius $b = R/H$. Curves are plotted for the same values of parameters as in Fig. 3. Flux in is shown in dimensionless units on the right-hand ordinate. (*A*) Flux for an extensive range of pore radii. (*B*) Flux for narrow pores only.

from macromolecular structures, such as interactions of adhesion between cytoskeleton and membrane. The lower end, $\eta_s \approx 10^{-7}$ g/s, is the measured microviscosity of the hydrocarbon interior of a bilayer membrane (Azzi, 1975) and corresponds to $\eta_3 \approx 1$ poise, the viscosity of olive oil. The same η_s's were obtained by measuring electrically induced expansion of pores in lipid bilayers formed in *n*-decane (Sukharev et al., 1983); these values reflect all of the molecular interactions within a monolayer, that is, due to both lipids and organic solvent. Estimates of η_s for biological membranes that are based on measurements of lateral diffusion give $\eta_s \approx 10^{-6}$ to 10^{-5} g/s (for reviews, see Evans and Hochmuth, 1978; Saffman, 1976; Thomas and Webb, 1990). As these viscosities characterize movement of lipid within a cell membrane without deformation of the membrane itself and account for both lipid-lipid and lipid-protein friction, we consider these latter values of η_s to be most descriptive of the in-plane lipid flow within cell membranes.

In contrast to η_s, experimental data that determine the relative viscosity η_r are rather limited. A value of η_r for pure lipid bilayers can be estimated from measurements of the dynamics of enlargement of hemifusion diaphragms (Melikyan et al., 1985). Outer monolayers, after initial merger, are pulled away from the site of hemifusion. This clearing of outer monolayers from the site allows the inner monolayers to come into direct apposition with each other, forming and enlarging into a hemifusion diaphragm. The time dependence of this expansion in area of the diaphragm, $S(t)$, is governed by tension and friction between monolayers. $S(t)$ is described by the equation (Kumenko et al., 1999)

$$S(t) = S_0 + \frac{4\pi\sigma h^2}{\eta_r(2\ln(R_m/R_0) + 1)}\, t \qquad (22)$$

where R_0 is the radius of the diaphragm at the moment the expansion is monitored and R_m is the radius of the fusing bilayer. A comparison of the actual initial slope, dS/dt, to that obtained from Eq. 22 yields the viscosity η_r. Experimentally, the rate of area expansion of the diaphragm, dS/dt, was 1.1×10^{-4} cm^2/s for phosphatidylethanolamine (PE) ($2\sigma = 1.2$ dyn/cm) membranes and was 0.7×10^{-4} cm^2/s for asolectin (AS) ($2\sigma = 0.5$ dyn/cm) membranes in *n*-decane (Melikyan et al., 1985). When these values are combined with the known geometrical parameters, $R_0 \approx 10^{-2}$ cm and $R_m \approx 10^{-1}$ cm, Eq. 22 yields that $\eta_r \approx 6 \times 10^{-10}$ g/s for PE and $\eta_r \approx 4 \times 10^{-10}$ g/s for AS. This two-dimensional viscosity η_r scaled with $h = 2$ nm yields the three-dimensional viscosity, $\eta_3 \approx 3 \times 10^{-3}$ g/cm · s, rather close to the viscosity of *n*-decane, 8×10^{-3} g/cm · s. This probably occurs because appreciable amounts of *n*-decane reside between the lipid monolayers (White, 1977). The same analysis and experiments yield that the two-dimensional viscosity η_r for a "dry" solvent-free bilayer formed from PE in squalene is almost two orders of magnitude higher, $\sim 7 \times 10^{-8}$ g/s.

The frictional interactions between monolayer leaflets as they slip past each other have also been studied by pulling tethers out of lipid vesicles (Merkel et al., 1989; Evans et al., 1992; Evans and Young, 1994; Raphael and Waugh, 1996). When normalized to a monolayer thickness of $h = 2$ nm, η_r was found to be between $\sim 4 \times 10^{-7}$ g/s (Evans and Young, 1994) and $\sim 1.8 \times 10^{-6}$ g/s (Raphael and Waugh, 1996). The higher values of η_r deduced for the vesicular membrane than for bilayers in *n*-decane arise because of a lack of the "lubricating" *n*-decane between the monolayer leaflets of vesicles. Although the data indicate that η_s may be somewhat larger than η_r for purely lipidic bilayers, on balance we can take $\eta_r \approx \eta_s$, each in the range of 10^{-5} to 10^{-6} g/s. However, in some cases viscosity has been measured to be significantly larger: pulling microtethers out of neuronal growth cone membranes yielded $\eta \approx 2 \times 10^{-4}$ g/s (Dai and Sheetz, 1995b). It is not clear why slippage of monolayers past each other leads to such a high value of viscosity. In our subsequent comparison of theory with experiments, we assume that $\eta_r \approx \eta_s$ also holds for cell membranes, within the interval 10^{-5} to 10^{-6} g/s.

We have ignored in our analysis the friction between water and lipid at the water-membrane interface. We justify this simplification, showing that this friction is negligible for pores with either a wide or narrow lumen. For ease of calculation, we treat a large pore's wall as if its circumference were straight rather than curved (in other words, as if the circle that forms the lumen were cut open and the ends separated so that they form the ends of a semicylinder). That is, we approximate a large pore as a semicylinder of radius H that joins two parallel semiinfinite planar membranes separated by a distance $2H$. The axis of this semicylinder runs parallel to the planar membranes. At the surfaces of the planar membranes the difference between the velocity of water and lipid flow is zero, the "no-slip condition"; sufficiently far from the surface the water velocity is zero, and the difference in velocity is therefore the lipid velocity v, given by Eq. 20. The solutions for the frictional force per unit length, F (dyn/cm), are well known for a liquid moving past both a flat plate and a cylinder (Landau and Lifshitz, 1987). Combining these two solutions, we obtain

$$F = 1.3 \cdot \sqrt{\eta_w \rho_w R_m v^3} + \frac{2\pi\eta_w v}{\ln(3.7(\eta_w/Hv\rho_w))} \qquad (23)$$

where the first term corresponds to a planar part and the second one to the semicylinder. η_w is the dynamical viscosity of water, ρ_w is the water density, and R_m is a characteristic length of the system which, as an upper bound, can be taken as $R_m \approx 1$ mm. To estimate the maximum force F generated by lipid-water friction, we consider a huge pore under a large tension difference, 1 dyn/cm. The maximum lipid velocity is ~5 mm/s (see Fig. 3) when the membrane viscosity is at a minimum, 10^{-6} g/s. Even for this maximum velocity, both terms in Eq. 23, $\sim 10^{-3}$ dyn/cm, are much smaller than the tension difference of 1 dyn/cm. Therefore water-membrane friction gives a negligibly small correction in the case of large pores.

For a small pore, both the velocity gradient of the water and the momentum transfer to the pore wall are high. But as the area of the pore wall is small, lipid-water friction is negligible in this case as well. The frictional force for a unit length of pore circumference, F_p (units dyn/cm), can be estimated as

$$F_p \approx \eta_w \frac{\partial v}{\partial r} 2H \approx \eta_w \frac{v}{r_p} 2H \qquad (24)$$

where v is the characteristic lipid velocity. From Fig. 3 *B*, for a pore with a radius of ~1 nm, $v \approx 10^{-2}$ cm/s for $\Delta\sigma \approx 1$ dyn/cm and $\eta \approx 10^{-6}$ g/s. Equation 24 yields $F_p \approx 10^{-3}$ dyn/cm $\ll 1$ dyn/cm.

Comparison of energy dissipation due to shear and relative viscosities

As steady-state lipid velocity and flux are set by energy dissipation, it is useful to explicitly consider the two dissi-

pative viscous processes. Under the assumption $\eta_s = \eta_r = \eta$, the comparative contributions of the two processes to overall energy dissipation are determined by the form factors $I(b)$ and $J(b)$. Fig. 2 shows that over the entire range of biologically interesting pore radii, $r_p < 35$ nm, shear deformation dominates relative friction in causing dissipation. If $\eta_s > \eta_r$, the dominance becomes greater. The integrands of $I(b)$ and $J(b)$ of Eqs. 14 and 18′ (Fig. 5) characterize the distribution of energy dissipation along the pore wall as a function of the angle φ.

For small pores ($r_p < 10$ nm), shear dissipation essentially arises in the toroidal region: the contribution to $I(b)$ from the planar membrane is 2 and $I(b) \gg 2$. The origins of shear deformation within the pore and planar membrane are straightforward. Within the planar membrane, flow is only radial, and shear occurs because any element of membrane area becomes progressively shorter in the radial direction as it moves further from the pore. Within the pore, membrane undergoes shear deformation in regions where the pore wall is curved. If a region of a pore wall is perfectly cylindrical, membrane does not deform as it moves along this portion of the wall, regardless of the size of the cylindrical lumen. In general, flow of an element of membrane area parallel to the axis of symmetry occurs without shear deformation; flow perpendicular to the axis results in maximum deformation. We can thus appreciate why shear dissipation is distributed nonhomogeneously through the pore wall (Fig. 5). In the center of the pore, $\varphi = 0$, the wall is locally cylindrical, and hence $I(b) = 0$. As material moves away from the center of the pore, flow occurs progressively more perpendicular to the symmetry axis and shear deformation increases, accounting for the increases in $I(b)$. But as the element of membrane area moves further from the symmetry axis, the deformation due to radial shortening lessens. This competition in shear deformation between radial and angular positioning of a membrane element leads to maxima in $I(b)$, symmetrically placed around $\varphi = 0$. For a toroid, the maxima are at $|\varphi| \approx 0.5$; beyond this value shear deformation gradually decreases to the level of the planar membrane.

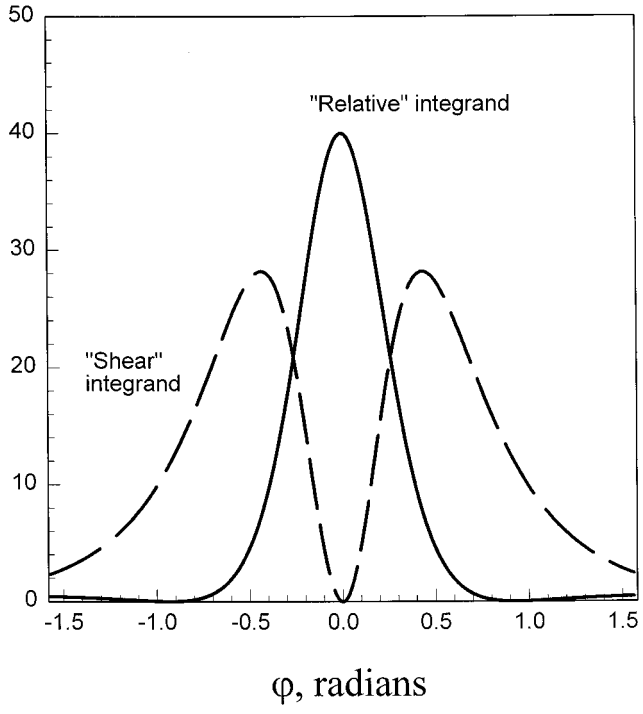

FIGURE 5 Energy dissipation density along the pore wall. The dashed curve is the integrand of $\tilde{I}$ (Eq. 14) and represents shear friction; the solid curve is the integrand of J (Eq. 18′) and provides the relative friction. The values of these integrands as functions of φ allow the contribution of the two forms of dissipation to be compared for any portion of membrane within the pore. The curves are plotted for $H = 10$ nm, $h = 2$ nm, and $b = 1.2$ (i.e., $r_p = 0$).

For relative viscosity, the integrand of $J(b)$ reaches a maximum at $\varphi = 0$, with relatively narrow dispersion, demonstrating that dissipation due to monolayers slipping past each other is concentrated in a narrow region near the pore neck. Physically this occurs because, by the principle of continuity, the same flux of lipid must pass through the inner and outer monolayers for every angle φ. The circumferences of outer and inner monolayers (around the central symmetry axis of the pore) are smallest at the narrow pore neck. As a result, the difference in velocity and thus in energy dissipation is greatest at the pore neck. The geometric factor $J(b)$ is large for the smallest pores and decreases as r_p increases (Fig. 2, Table 1): the larger the pore, the more the circumferences of the inner and outer monolayers become comparable, and differences in monolayer velocities become smaller. This decrease in $J(b)$ with pore growth is opposed by the fact that the sliding occurs along a larger pore circumference, a circumference that increases linearly with r_p. When the pore enlarges sufficiently, beyond $r_p \approx H$, this latter effect begins to dominate (hence there is a minimum in $J(b)$) and $J(b)$ increases roughly linearly with pore radius. $J(b)$ is greater than $I(b)$ after $r_p \approx 30$ nm, at which stage pores have enlarged immensely.

If we view a fusion pore as a long cylinder connected to each of the fused membranes at a region that curves back into the plane of the membrane, we can qualitatively evaluate energy dissipation due to flow. Shear would not occur within the cylindrical region, but would within the curved portions (which we refer to as “dimples”). In contrast to the pattern of shear deformation, intermonolayer friction would occur predominantly within the cylindrical pore. That is, if the neck of the pore were elongated, shear dissipation would not be affected, but relative dissipation would be augmented. In other words, pore geometries other than toroidal should lead to similar energy dissipations for the same lumen dimensions. Thus, Eqs. 20 and 21 for lipid velocity and flux can be used to describe experimental data, even though the true pore shape is not known.

Lipid velocity and area flux

Lipid velocity, $v(b)$, levels (Fig. 3 *A*) and the area flux, $\Phi(b)$, increase linearly (Fig. 4 *A*) with radius as $b \rightarrow \infty$. The

physical basis of these functions can be appreciated by realizing that when $R \gg H$, dissipation is dominated by intermonolayer friction (i.e., $J(b) > I(b)$ for extremely large pores; Fig. 2). The rate of intermonolayer dissipation increases linearly with radius R but quadratically with v; the rate of work done by tension increases linearly with both radius and v. It follows immediately from the equality of dissipation and rate of work done by tension that velocity is independent of radius (equivalently, see Eq. 20 and the asymptotic expression for $J(b)$ in Table 2). As $\Phi = 2\pi R \cdot v$, a constant v means Φ increases linearly with R for large pores.

For small pores, lipid velocity increases in a greater than linear manner with increases in r_p (Fig. 3 *B*). However, balancing the energy dissipated in the planar membranes by the work performed by tension yields only a linear increase in lipid velocity. The overall nonlinearity is due to geometric effects of the fusion pore (Table 2), which arise because the curved pore wall induces shear dissipation, and a narrow neck leads to significant relative, intermonolayer dissipation (Figs. 2 and 5). Both dissipations should occur for small pores, independent of the specific geometry. Hence, the slope of the curve of v versus r_p (dv/dr_p) increases with r_p for small pores (Fig. 3 *B*).

Lipid flux depends on the difference in tension between the two membranes, $2\Delta\sigma$, regardless of the precise geometry of the pore. This is of practical importance: it is not necessary to know how the tension difference drops along the walls of the pore to calculate flux. As a consequence, a simple equation, Eq. 21, can be used to describe experimental flux data.

A test of the physics of lipid movement

To determine whether the present model accurately describes lipid flow for homogeneous membranes that have merged requires flux data for a system in which the parameters (η, R, and $\Delta\sigma$) have been measured. This has not yet been done experimentally. But the validity of our picture of the physics underlying lipid flow is testable. Two bulged solvent-free planar bilayers with different percentages of charged lipids could be hemifused, and the lipid flux between the merged monolayers could be determined accurately by measuring the change in surface potential of the nonhemifused portions of the planar membranes (Chernomordik et al., 1987). The viscosity and tension of the bilayer of each lipid composition would be obtained independently by standard techniques (Chernomordik et al., 1987). A straightforward modification of the present theory to the case of lipid flow during hemifusion in a system whose geometry was unambiguously known will provide a severe test of our approach. However, we can immediately apply the present theory to experiments for which lipid flux has been measured through enlarged pores.

Comparison of the theory with experiment

Fluorescent lipid dye has not been observed to pass through small fusion pores (less than ~400 pS) connecting influenza hemagglutinin (HA)-expressing cells to RBCs (Tse et al., 1993; Zimmerberg et al., 1994). This apparent exclusion of lipid has been taken as evidence that these pores are composed solely of protein (Tse et al., 1993), implying that hemifusion is not an intermediate step in membrane fusion. However, the finding that fusion pore formation depends on the constituent membrane lipids contradicts this conclusion (Chernomordik et al., 1997, 1998). These latter findings strongly support the view that lipids are intimately involved in pore formation, rather than incorporating into the pore after formation. All of the experimental findings could be accounted for if both protein and lipid were intimately involved not only in the formation, but also the structure, of the initial pores. Multiple fusion proteins act cooperatively to form a pore, and even if these proteins induce fusion through a hemifusion mechanism, they may form a tight ring of protein that significantly inhibits lipid flux (Hernandez et al., 1996; Chernomordik et al., 1998). The theory of convection does not apply to the case of small pores connecting HA-expressing cells to RBCs, for at least two reasons. First, if a ring of protein inhibits lipid flux, the membrane of the pore wall is heterogeneous, rather than homogeneous. Second, as the in-plane tension of cell membranes is small, their difference is negligible; the hindered transport across the pore would be governed by passive diffusion, not by convection. The theory of the present paper can, however, be directly applied when differences in membrane tension cause lipids to flow between fused membranes.

When cells expressing the hemagglutinin of influenza virus are fused to planar lipid bilayers, a substantial amount of lipid flows from the cell to the planar membrane after full pore enlargement (Melikyan et al., 1995). This flux was measured by including the fluorescent dye octadecylrhodamine in the planar membrane. After a fusion pore expanded to large conductances, with a mean value of ~500 nS (Melikyan et al., 1993) (i.e., $r_p \approx 500$ nm), a dark spot in fluorescence was observed at the site of the fusing cell. Darkening occurred only after full pore enlargement. The dark spot then expanded (up to a radius of ~20 μm), maintaining a rather sharp boundary. The darkening is accounted for by the tension of the planar membrane as it pulls on the membrane of the fused cell; unlabeled lipid in the cell membrane flows into the planar membrane, thereby displacing fluorescent lipid molecules with nonfluorescent ones. Experimentally, the initial area flux is between 5×10^{-6} and 7×10^{-6} cm^2/s (Razinkov, Melikyan, and Cohen, unpublished data). This flux approaches zero after ~2 s, in accord with the tension of the cell membrane, after fusion, drawn to that of the planar membrane. We compare Eq. 21 with the initial flux because we can estimate the initial value of $2\Delta\sigma$. The initial in-plane tension of the cell membrane is small, $\sim 10^{-2}$ dyn/cm; we take the tension of the planar

membrane (PE/PC, 2:1) as $2\sigma \approx 1$ dyn/cm (Chernomordik et al., 1987). If we let $\eta_s \approx \eta_r = \eta$ and introduce $\Phi_m = \Phi/2$ as the area flux for one monolayer, we rewrite Eq. 21 as

$$\eta = \frac{\pi \Delta\sigma b^2 H^2}{\Phi_m[I(b) + J(b)]}$$

For $H = 10$ nm, $b = R/H = 50$ (i.e., a fully enlarged pore of $r_p \approx 500$ nm), we obtain $[I(b) + J(b)] = 41$ (Table 2). The measured $\Phi_m = 6 \times 10^{-6}$ cm^2/s implies that $\eta = 1.5 \times 10^{-5}$ g/s, in reasonable accord with the expectation that membrane viscosities lie within the interval 10^{-6} to 10^{-5} g/s.

In addition to the convective flux of the unlabeled lipid from the cell into the planar membrane, the fluorescent dye diffuses from the planar bilayer to cell membrane. Diffusion will cause the front of darkening—which would be sharp if only convection were present—to spread out with time. This broadening of the front is given by $(2D\tau)^{1/2}$, where D is the diffusion constant of the lipid dye, $\sim 10^{-8}$ cm^2/s. The observed spread of darkening occurs over a time course of $\tau \approx 2$ s (Razinkov, Melikyan, and Cohen, unpublished data), and thus the diffusive spread is ~ 2 μm, much smaller than the radius of the enlarged dark area (~ 20 μm). That is, diffusive flux is relatively small compared to convective flux; the boundary of the dark spot remains relatively sharp.

The situation is quite different for small pores. For $r_p \approx 1$ nm ($R = 13$ nm), theoretically the convective flux of the dye (~ 5 mol% of lipid in the planar bilayer) is $\sim 4 \times 10^5$ molecules/s (Fig. 4 *B*; using an area per lipid of 5×10^{-15} cm^2 to convert area flux in units of cm^2/s to units of molecules/s). To estimate the diffusive flux, we treat the small fusion pore as a cylinder with radius 7 nm and length $l = 2H = 20$ nm and obtain a diffusive flux of $\sim 4 \times 10^5$ molecules/s (i.e., the convective and diffusive fluxes are comparable). This is in agreement with experiment (Melikyan et al., 1995): for small flickering pores, a darkening of the planar membrane is not observed, but a brightening of the cell occurs.

We can also apply our equations to the case of tension-driven lipid flux between secretory granules and plasma membrane in mast cell secretion (Monck et al., 1990; Oberhauser and Fernandez, 1993). From capacitance measurements, $\sim 1.5 \times 10^{-9}$ cm^2/s of plasma membrane (or 6×10^5 lipids/s) moves into granule membrane while a transient fusion pore is open, suggesting that the tension of granules is higher than that of plasma membrane. The total flux was proportional to the time the transient pore remained open, implying that the tension difference remained constant. (The lipid flux in these experiments was about three orders of magnitude less than for the case of cells fused with planar membranes. This probably accounts, in large part, for the fact that the difference in tension between plasma and granule membranes does not relax to zero.) Based on conductances expected of transient (flickering) fusion pores, the pore radius can be estimated as $r_p \approx 1$ nm. Using Eq. 21′, the geometrical factors $I(b)$, $J(b)$ (Table 1), and viscosity, $\eta \approx 10^{-5}$ g/s (as determined from the measured lipid flux between fused cells and planar membranes), we obtain that the tension difference between granule and plasma membrane, $\Delta\sigma$, is ~ 0.1 dyn/cm. This indicates that the granule membrane probably has significantly higher in-plane tension than a plasma membrane. The membranes of Golgi and ER also exhibit high tensions (Sciaky et al., 1997); it may be that intracellular membranes generally exhibit higher tensions than plasma membranes because of differences in chemical potential.

In summary, the present theory provides a means for understanding the physics of lipid flow through fusion pores. While the specific compositions and geometric structures of fusion pores are not yet known, in this paper we have derived equations that can be employed to interpret, in a practical manner, experimentally obtained lipid fluxes between membranes under different tensions.

APPENDIX A: THE COORDINATE SYSTEMS

To calculate the velocity distribution and rate of energy dissipation in the planar portions of the membranes, we use cylindrical coordinates (r, θ, z). These coordinates are related to Cartesian coordinates (Fig. 1 *B*) by

$$\begin{cases} x = r\cos\theta \\ y = r\sin\theta \\ z = z \end{cases} \tag{A1}$$

Differential operators and the viscous stress tensor are transformed from Cartesian to curvilinear coordinates through the Lamé coefficients (Korn and Korn, 1968)

$$H_i = \sqrt{\left(\frac{\partial x}{\partial i}\right)^2 + \left(\frac{\partial y}{\partial i}\right)^2 + \left(\frac{\partial z}{\partial i}\right)^2} \tag{A2}$$

In cylindrical coordinates, $i = r, \theta, z$. Substituting Eq. A1 into Eq. A2 yields

$$H_r = 1, \quad H_\theta = r, \quad H_z = 1 \tag{A3}$$

An element of area is

$$dS = d\theta \cdot r\, dr \tag{A4}$$

The radial flow in the planar portions of the membranes depends on r only, $v_\theta = 0$, $v_z = 0$, $v_r \neq 0$. The components of the viscous stress tensor can be written as

$$\sigma_{rr} = 2\eta\frac{\partial v_r}{\partial r}, \quad \sigma_{\theta\theta} = 2\eta\frac{v_r}{r}, \quad \sigma_{zz} = \sigma_{r\theta} = \sigma_{\theta z} = \sigma_{rz} = 0 \tag{A5}$$

The system of coordinates ρ, φ, θ within the toroidal pore (Fig. 1) is

$$\begin{cases} x = (R - \rho\cos\varphi)\cos\theta \\ y = (R - \rho\cos\varphi)\sin\theta \\ z = \rho\sin\varphi \end{cases} \tag{A6}$$

Substituting Eq. A6 into Eq. A2 for $i = \rho, \varphi, \theta$, we obtain

$$H_\rho = 1, \quad H_\varphi = \rho, \quad H_\theta = R - \rho\cos\varphi \tag{A7}$$

For an element of area we have

$$H_\rho = 1, \quad H_\varphi = \rho, \quad H_\theta = R - \rho\cos\varphi \tag{A8}$$

A radius $r(\varphi)$ from the z axis of the pore to any point on the circumference of the toroidal surface is

$$r(\varphi) = R - \rho\cos\varphi \tag{A9}$$

For a velocity distribution $v_\rho = 0$, $v_\varphi \neq 0$, $v_\theta = 0$ ($v = v_\varphi$ depends on φ only), the components of the viscous stress tensor have the form

$$\sigma_{\rho\rho} = 0, \quad \sigma_{\varphi\varphi} = 2\eta\frac{1}{\rho}\frac{\partial v_\varphi}{\partial\varphi},$$

$$\sigma_{\theta\theta} = 2\eta\frac{v_\varphi\sin\varphi}{R-\rho\cos\varphi}, \quad \sigma_{\rho\varphi} = \sigma_{\rho\theta} = \sigma_{\varphi\theta} = 0 \tag{A10}$$

APPENDIX B: THE GENERAL EXPRESSIONS FOR LIPID VELOCITY WITHOUT THE ASSUMPTION THAT $v' = v''$

Energy dissipation

To justify the approximation $v' = v''$ used in the main body of the paper, we present the exact expressions for each of the terms of the energy dissipation in Eq. 10. We obtain these expressions from Eqs. 3, 11, and 15:

$$\dot{E}_{st} = 2\pi\eta_s\tilde{I}(b)(v_+^2 + v_-^2) \tag{B1}$$

where

$$\tilde{I}(b) = 2\int_{-\pi/2}^{\pi/2}\frac{b^2\sin^2\varphi\,d\varphi}{(b-\cos\varphi)^3}, \quad b = \frac{R}{H}$$

$$v_+ = v' + v'', \quad v_- = v' - v''$$

$$\dot{E}_{r\pi} = 2\pi\eta_r J(b)v_+^2 + 2\pi\eta_r\left[\frac{H}{h}J^{\pm}(b)v_+v_- + \frac{H^2}{h^2}J^-(b)v_-^2\right] \tag{B2}$$

and

$$J(b) = \frac{1}{2}\int_0^{\pi/2}\frac{b^2(b-2\cos\varphi)^2}{(b-\cos\varphi)^3}\,d\varphi$$

$$J^{\pm}(b) = \int_0^{\pi/2}\frac{b^2(b-2\cos\varphi)^2}{(b-\cos\varphi)^2}\,d\varphi$$

$$J^-(b) = 2\int_0^{\pi/2}\frac{b^2}{b-\cos\varphi}\,d\varphi$$

$$\dot{E}_{sp} = 4\pi\eta_s(v_+^2 + v_-^2) \tag{B3}$$

In the case of $v' \neq v''$ an additional term appears because of the relative friction between monolayers moving past each other within the planar membranes:

$$\dot{E}_{rp} = \frac{4\pi\eta_r}{h^2}R^2v_-^2\ln\frac{R_m}{R} \tag{B4}$$

By adding each of the individual terms for energy dissipation (Eqs. B1–B4), we obtain the total energy dissipation rate $\dot{E}$.

Lagrange's equation with a dissipation function, F

The fusion system is described by two time-dependent variables v' and v'' or, equivalently, v_+ and v_- (see Eq. B1). The equations of motion can be described by Lagrange's equations with dissipation in the system (Goldstein, 1950), which in our notation has the form

$$\frac{\partial W_\sigma}{\partial l_{+,-}} = \frac{\partial F}{\partial v_{+,-}}, \tag{B5}$$

where $l_{+,-}$ are the generalized coordinates associated with the velocities $v_{+,-}$ (i.e., $v_{+,-} = dl_{+,-}/dt$), W_σ is the work done by the tensions $2\sigma_1$ and $2\sigma_2$, and F is the dissipation function. Equation B5 reflects the fact that the work performed by external forces is balanced by viscous dissipation. As W_σ does not explicitly depend on time, we obtain

$$\dot{W}_\sigma = \frac{dW_\sigma}{dt} = \frac{\partial W_\sigma}{\partial l_+}v_+ + \frac{\partial W_\sigma}{\partial l_-}v_-. \tag{B6}$$

Directly calculating $\dot{W}_\sigma$ for the case $v' \neq v''$ yields

$$\dot{W}_\sigma = 2\pi R\Delta\sigma\cdot v_+ \tag{B7}$$

and, hence, from Eqs. B6 and B7 we obtain

$$\begin{cases}\dfrac{\partial W_\sigma}{\partial l_+} = 2\pi R\Delta\sigma\\[2ex] \dfrac{\partial W_\sigma}{\partial l_-} = 0\end{cases} \tag{B8}$$

The energy dissipation rate $\dot{E}$ and dissipation function F are related by $2F = \dot{E}$ (Goldstein, 1950), resulting in

$$F = \pi[\eta_r I(b) + \eta_s J(b)] + \pi\eta_r\left[\frac{H}{h}J^{\pm}(b)v_+v_- + \frac{H^2}{h^2}\tilde{J}^-(b)v_-^2\right] \tag{B9}$$

where $I(b) = 2 + \tilde{I}(b)$, $\tilde{J}^-(b) = J^-(b) + 2b^2\ln(b_m/b)$, $b_m = R_m/H$.

From Eqs. B6, B8, and B9 we obtain

$$v_+ = \frac{\Delta bH}{[\eta_r I(b) + \eta_s J(b)][1 - K(b)]} \tag{B10}$$

where

$$K(b) = \frac{[J^{\pm}(b)]^2}{4J^-\left[\dfrac{\eta_r}{\eta_s}I(b) + J(b)\right]}$$

and

$$v_- = -\frac{h}{H}\cdot\frac{J^{\pm}(b)}{2\tilde{J}^-(b)}v_+ \tag{B11}$$

Numerical calculation shows that $|K(b)| < 3\times10^{-2}$, allowing $K(b)$ to be neglected in the denominator of Eq. B10. Equation B10 therefore reduces to

$$v_+ = \frac{\Delta\sigma bH}{\eta_r I(b) + \eta_s J(b)}. \tag{B12}$$

Equation B11 for v_- can be simplified for the case $R_m \gg R$ (or $b_m \gg b$) by noting that from the definition of $\tilde{J}^-(b)$ (Eq. B9), the second term

dominates for large b_m. Dropping the first term, i.e., $\tilde{J}^-(b) \approx 2b^2 \ln b_m/b$, allows Eq. B11 to be written as

$$v_- \approx \frac{h}{H}\frac{1}{\ln(b_m/b)}\frac{J^{\pm}(b)}{4b^2}v_+ \qquad \text{(B13)}$$

Numerical calculations show that $J^{\pm}(b)/4b^2 < 0.4$ for all b. Taking $R_m \approx 10\ \mu$m, $h \approx 2$ nm, and $H \approx 10$ nm, we obtain for 1 nm $\leq r_p \leq$ 100 nm

$$v_- \approx 2 \times 10^{-2} \cdot v_+ \ll v_+ \qquad \text{(B14)}$$

Thus the contribution of v_- to the dissipation function F is negligible. Assuming that $v' = v''$ leads to a relative error in v_+ of less than 2% if $R_m > 10\ \mu$m. In other words, $v' = v'' = v$ is an excellent approximation for $R_m \gg R$.

We thank Drs. E. Evans, V. Frolov, S. Leikin, G. Melikyan, and A. Parsegian for useful discussions and suggestions. This work was supported in part by Fogarty International Research Collaboration Award R03 TW00715, National Institutes of Health grant GM27367, the Russian Foundation for Basic Research grant 94-04-50779, and the Soros Educational Program.

REFERENCES

Azzi, A. 1975. The application of fluorescent probes in membrane studies. *Q. Rev. Biophys.* 8:237–316.

Chandler, D. E., and J. E. Heuser. 1979. Membrane fusion during secretion. Cortical granule exocytosis in sea urchins studied by quick-freezing and freeze fracture. *J. Cell Biol.* 83:91–108.

Chanturiya, A., L. V. Chernomordik, and J. Zimmerberg. 1997. Flickering fusion pores comparable with initial exocytotic pores occurs in protein-free phospholipid bilayers. *Proc. Natl. Acad. Sci. USA.* 94: 14423–14428.

Chen, Yi-der, R. J. Rubin, and A. Szabo. 1993. Fluorescence dequenching kinetics of single cell-cell fusion complexes. *Biophys. J.* 65:325–333.

Chernomordik, L. V., V. Frolov, E. Leikina, P. Bronk, and J. Zimmerberg. 1998. The pathway of membrane fusion catalyzed by influenza hemagglutinin: restriction of lipids, hemifusion, and lipidic fusion pore formation. *J. Cell Biol.* 140:1369–1382.

Chernomordik, L. V., M. M. Kozlov, and J. Zimmerberg. 1995. Lipids in biological membrane fusion. *J. Membr. Biol.* 146:1–14.

Chernomordik, L. V., E. Leikina, V. Frolov, P. Bronk, and J. Zimmerberg. 1997. An early stage of membrane fusion mediated by the low pH conformation of influenza hemagglutinin depends upon membrane lipids. *J. Cell Biol.* 136:81–93.

Chernomordik, L. V., G. B. Melikyan, and Yu. A. Chizmadzhev. 1987. Biomembrane fusion: a new concept derived from model studies using two interacting planar lipid bilayers. *Biochim. Biophys. Acta.* 906: 309–352.

Cohen, F. S., M. H. Akabas, J. Zemmerberg, and A. Finkelstein. 1984. Parameters affecting the fusion of unilamellar phospholipid vesicles with planar bilayer membranes. *J. Cell Biol.* 98:1054–1062.

Curran, M. J., F. S. Cohen, D. E. Chandler, P. J. Munson, and J. Zimmerberg. 1993. Exocytotic fusion pores exhibit semi-stable states. *J. Cell Biol.* 133:61–75.

Dai, J., and M. P. Sheetz. 1995a. Regulation of endocytosis, exocytosis, and shape by membrane tension. *Cold Spring Harb. Symp. Quant. Biol.* 60:567–571.

Dai, J., and M. P. Sheetz. 1995b. Mechanical properties of neuronal growth cone membranes studied by tether formation with laser optical tweezers. *Biophys. J.* 68:988–996.

Deryaguin, B. V., and Yu. V. Gutop. 1962. The theory of the rupture of free films. *Kolloidniy J.* 24:431–437 (in Russian).

Deryaguin, B. V., and A. V. Prokhorov. 1981. On the theory of the rupture of black films. *J. Colloid Interface Sci.* 81:108–115.

Einstein, A. 1956. A new determination of molecular dimensions. *In* Translation in Investigations on the Theory of the Brownian Movement. R. Fürth, editor. Dover Publications, New York. 36–62.

Evans, E. A., and R. M. Hochmuth. 1978. Mechanochemical properties of membranes. *Curr. Top. Membr. Transp.* 10:1–62.

Evans, E. A., and R. Skalak. 1980. Mechanics and Thermodynamics of Biomembranes. CRC Press, Boca Raton, FL. 1–254.

Evans, E. A., and A. Young. 1994. Hidden dynamics in rapid changes in bilayer shape. *Chem. Phys. Lipids.* 73:39–56.

Evans, E. A., A. Young, R. E. Waugh, and J. Song. 1992. Dynamic coupling and nonlocal curvature elasticity in bilayer membranes. *In* The Structure and Conformation of Amphiphilic Membranes. R. Lipowsky, D. Richter, and K. Kremer, editors. Springer-Verlag, Berlin. 148–153.

Goldstein, H. 1950. Classical Mechanics. Addison-Wesley, Reading, MA.

Helfrich, W. 1973. Elastic properties of lipid bilayers: theory and possible experiments. *Z. Naturforsch.* C28:693–703.

Hernandez, L. D., L. R. Hoffman, T. G. Wolfsberg, and J. M. White. 1996. Virus-cell and cell-cell fusion. *Annu. Rev. Cell Dev. Biol.* 12:627–661.

Knoll, G., C. Braun, and H. Plattner. 1991. Quenched flow analysis of exocytosis in *Paramecium* cells: time course, changes in membrane structure, and calcium requirements revealed after rapid mixing and rapid freezing of intact cells. *J. Cell Biol.* 113:1295–1304.

Kumenko, D. A., P. I. Kuzmin, and Yu. A. Chizmadzhev. 1999. Lipid flux during expansion of a trilaminar structure. *Biologicheskie Membrany.* (in press) (in Russian).

Korn, G. A., and T. M. Korn. 1968. Mathematical Handbook, 2nd ed. McGraw-Hill, New York.

Landau, L. D., and E. M. Lifshitz. 1987. Fluid Mechanics, 2nd ed. Pergamon Press, Oxford.

Lindau, M., and W. Almers. 1995. Structure and function of fusion pores in exocytosis and ectoplasmic membrane fusion. *Curr. Opin. Cell Biol.* 7:509–517.

Markin, V. S., M. M. Kozlov, and V. L. Borovjagin. 1984. On the theory of membrane fusion. The stalk mechanism. *Gen. Physiol. Biophys.* 5:361–377.

Melikyan, G. B., L. V. Chernomordik, and I. G. Abidor. 1985. Surface area expansion for trilaminar structure during monolayer membrane fusion. *Biologicheskie Membrany.* 2:1048–1054 (in Russian; English translation in *Biological Membranes*, Vol. 2. Harwood Academic Publishers, 1998, pp. 1865–1876).

Melikyan, G. B., W. D. Niles, M. E. Peeples, and F. S. Cohen. 1993. Influenza hemagglutinin-mediated fusion pores connecting cells to planar membranes: flickering to final expansion. *J. Gen. Physiol.* 102: 1131–1149.

Melikyan, G. B., J. M. White, and F. S. Cohen. 1995. GPI-anchored influenza hemagglutinin induces hemifusion to both red blood cell and planar bilayer membranes. *J. Cell Biol.* 131:679–691.

Merkel, R., E. Sackmann, and E. A. Evans. 1989. Molecular friction and epitatic coupling between monolayers in supported bilayers. *J. Phys. France.* 50:1535–1555.

Monck, J. R., G. A. de Toledo, and J. M. Fernandez. 1990. Tension in secretory granule membranes causes extensive membrane transfer through the exocytotic fusion pore. *Proc. Natl. Acad. Sci. USA.* 87: 7804–7808.

Nagle, J. F., and D. A. Wilkinson. 1978. Lecithin bilayers. Density measurements and molecular interactions. *Biophys. J.* 23:159–175.

Nanavati, C., V. S. Markin, A. F. Oberhauser, and J. M. Fernandez. 1992. The exocytotic fusion pore modeled as a lipidic pore. *Biophys. J.* 63:1118–1132.

Niles, W. D., J. R. Silvius, and F. S. Cohen. 1996. Resonance energy transfer imaging of phospholipid vesicle interaction with a planar phospholipid membrane. *J. Gen. Physiol.* 107:329–351.

Oberhauser, A. F., and J. M. Fernandez. 1993. Patch clamp studies of single intact secretory granules. *Biophys. J.* 65:1844–1852.

Ornberg, R. L., and T. S. Reese. 1981. Beginning of exocytosis captured by rapid-freezing of *Limulus* amebocytes. *J. Cell Biol.* 90:40–54.

Prigogine, I. 1967. Introduction to Thermodynamics of Irreversible Processes. John Wiley, New York.

Raphael, R. M., and R. E. Waugh. 1996. Accelerated interleaflet transport of phosphatidylcholine molecules in membranes under deformation. *Biophys. J.* 71:1374–1388.

Razinkov, V. I., G. B. Melikyan, R. M. Epand, R. F. Epand, and F. S. Cohen. 1998. Effects of spontaneous bilayer curvature on influenza virus-mediated fusion pores. *J. Gen. Physiol.* 112:409–422.

Rubin, R. J., and Yi-der Chen. 1990. Diffusion and redistribution of lipid like molecules between membranes in virus-cell and cell-cell fusion systems. *Biophys. J.* 58:1157–1168.

Ryan, T. A., H. Reuter, and S. J. Smith. 1997. Optical detection of a quantal presynaptic membrane turnover. *Nature.* 388:478–482.

Saffman, P. G. 1976. Brownian motion in thin sheets of viscous fluid. *J. Fluid. Mech.* 73:593–602.

Sciaky, N., J. Presley, C. Smith, K. J. Zaal, N. Cole, J. E. Moreira, M. Terasaki, E. Siggia, and J. Lippincott-Schwartz. 1997. Golgi tubule traffic and the effects of brefeldin A visualized in living cells. *J. Cell Biol.* 139:1137–1155.

Siegel, D. 1993. The energetics of intermediates in membrane fusion: comparison of stalk and inverted micellar intermediate mechanisms. *Biophys. J.* 65:2124–2140.

Solsona, C., B. Innocenti, and J. M. Fernández. 1998. Regulation of exocytotic fusion by cell inflation. *Biophys. J.* 74:1061–1073.

Südhof, T. C. 1995. The synaptic vesicle cycle: a cascade of protein-protein interactions. *Nature.* 375:645–653.

Sukharev, S. I., V. B. Arakelyan, I. G. Abidor, L. V. Chernomordik, and V. F. Pastushenko. 1983. Rupture of planar BLM under influence of electric field. *Biophysica.* 28:756–760 (in Russian).

Thomas, J. L., and W. W. Webb. 1990. Fluorescence photobleaching recovery: a probe of membrane dynamics. *In* Noninvasive Techniques in Cell Biology. J. K. Foskett and S. Grinstein, editors. Wiley-Liss, New York. 129–152.

Tien, H. Ti. 1974. Bilayer Lipid Membranes (BLM): Theory and Practice. Marcel Dekker, New York.

Tse, F. W., A. Jwata, and W. Almers. 1993. Membrane flux through the pore formed by a fusogenic viral envelope protein during cell fusion. *J. Cell Biol.* 121:543–552.

Waugh, R. E. 1982. Surface viscosity measurements from large bilayer vesicle tether formation. II. Experiment. *Biophys. J.* 38:29–37.

White, S. H. 1977. Studies of the physical chemistry of planar bilayer membranes using high-precision measurements of specific capacitance. *Ann. N.Y. Acad. Sci.* 303:243–265.

Zimmerberg, J., M. Curran, and F. S. Cohen. 1991. A lipid/protein complex hypothesis for exocytotic fusion pore formation. *Ann. N.Y. Acad. Sci.* 635:307–317.

Zimmerberg, J., R. Blumenthal, D. P. Sarkar, M. Curran, and S. J. Morris. 1994. Restricted movement of lipid and aqueous dyes through pores formed by influenza hemagglutinin during cell fusion. *J. Cell Biol.* 127:1885–1894.